Low-field vortex dynamics over seven time decades in a $Bi_2Sr_2CaCu_2O_{8+\delta}$ single crystal for temperatures $13 \leqslant T \leqslant 83$ K

M. Nideröst, A. Suter,* P. Visani, and A. C. Mota
Laboratorium für Festkörperphysik, Eidgenössische Technische Hochschule Zürich, 8093 Zürich, Switzerland

G. Blatter
Theoretische Physik, Eidgenössische Technische Hochschule Zürich, 8093 Zürich, Switzerland
(Received 6 November 1995)

Using a custom-made dc superconducting quantum interference device (dc-SQUID) magnetometer, we have measured the time relaxation of the remanent magnetization $M_{\rm rem}$ of a $Bi_2Sr_2CaCu_2O_{8+\delta}$ single crystal from the fully critical state for temperatures 13 K$\leqslant T \leqslant$83 K. The measurements cover a time window of seven decades 10^{-2} s$\leqslant t \leqslant 10^5$ s, so that the current density j can be studied from values very close to j_c down to values considerably smaller than j_c. From the data we have obtained (i) the flux-creep activation barriers U as a function of current density j, (ii) the current-voltage characteristics $E(j)$ in a typical range of 10^{-7}–10^{-15} V/cm, and (iii) the critical current density $j_c(0)$ at $T=0$. Three different regimes of vortex dynamics are observed: For temperatures $T \lesssim 20$ K the activation barrier $U(j)$ is logarithmic, no unique functional dependence $U(j)$ could be found for the intermediate-temperature interval 20 K$\leqslant T \lesssim$40 K, and finally for $T \gtrsim 40$ K the activation barrier $U(j)$ follows a power-law behavior with an exponent $\mu \simeq 0.6$. From the analysis of the data within the weak collective pinning theory for strongly layered superconductors, it is argued that for temperatures $T \lesssim 20$ K pancake vortices are pinned individually, while for temperatures $T \gtrsim 40$ K pinning involves large collectively pinned vortex bundles. A description of the vortex dynamics in the intermediate-temperature interval 20 K$\leqslant T \lesssim$40 K is given on the basis of a qualitative low-field phase diagram of the vortex state in $Bi_2Sr_2CaCu_2O_{8+\delta}$. Within this description a second peak in the magnetization loop should occur for temperatures between 20 and 40 K, as has been observed in several magnetization measurements in the literature.

I. INTRODUCTION

High-temperature superconductors (HTSC's) are characterized by large values of the Ginzburg-Landau parameter $\kappa = \lambda/\xi$, so that most of the H-T phase diagram is dominated by the presence of vortices. Furthermore, the high anisotropy of $Bi_2Sr_2CaCu_2O_{8+\delta}$ (Bi2212) has strong implications for the behavior of the flux lattice in the mixed state. When a magnetic field H is applied perpendicularly to the ab planes, the vortices can be described as two-dimensional ''pancake vortices''[1] lying in the superconducting CuO_2 layers. These pancake vortices interact both through the interlayer Josephson coupling and through electromagnetic coupling. Such a layered vortex structure is very sensitive to thermal and quantum fluctuations, especially considering the small coherence length ξ in the direction parallel to the CuO_2 planes. As a consequence, pinning is relatively weak as compared to classical type-II superconductors and strong relaxations of the magnetization M are observed[2–8] which deviate from a pure logarithmic time dependence.

Since the discovery of the HTSC's,[9] theoretical and experimental work concerning vortices and their dynamics has strongly intensified. Those investigations were mainly focused on a regime where the current density j is relatively small as compared to the critical current density j_c. Only little is known[10–12] at present regarding the vortex dynamics in a regime where the current density j is close to j_c.

In the work here, we investigate experimentally the low-field vortex dynamics in a Bi2212 single crystal for magnetic fields **H** perpendicular to the CuO_2 layers. For this purpose we have designed and constructed a dc superconducting quantum interference device (dc-SQUID) magnetometer with high sensitivity and long-time thermal stability. The measurements of the relaxation of the remanent magnetization $M_{\rm rem}$ are taken in the temperature interval 13 K$\leqslant T \leqslant$83 K and cover a time window of seven decades. The wide current range of the experimental data allows a detailed analysis of the vortex dynamics within the theoretical vortex-creep models.[13,14] Applying the method of Maley *et al.*[15] to the relaxation data, a characteristic functional dependence between the activation barrier U and the current density j is obtained for the temperature regimes $T \lesssim 20$ K and $T \gtrsim 40$ K, whereas for temperatures between 20 and 40 K the $U(j)$ relation is found to depend strongly on temperature. On the basis of a qualitative low-field phase diagram[16] of Bi2212, an interpretation of the behavior of the vortex dynamics in the temperature interval around the crossover temperature[17–20] $T \simeq 25$ K is given.

II. EXPERIMENTAL DETAILS

The measured single crystal is $0.9 \times 1.3 \times 0.05$ mm^3 in size, and the critical temperature T_c is 95 K, as determined by ac-susceptibility measurements. The growth procedure and the transport properties have been described elsewhere.[21] The experiments are performed in a custom-made dc-SQUID magnetometer, where the sample remains stationary in the pickup coil during the measurements. The externally applied

 © 1996 The American Physical Society

TABLE I. Maximum applied magnetic field H^{max} for different measuring temperatures T and values of the residual field H^{res}, which is due to the flux remaining trapped in the superconducting coil after the removal of the external field H. The residual field of the cryostat is about 10 mOe in opposite direction to the applied magnetic field.

T (K)	13	15–27	30–40	50	$\geqslant$60
H^{max} (Oe)	1500	1000	500	300	$<$100
H^{res} (mOe)	710$\pm$50	480$\pm$50	60$\pm$10	20$\pm$10	$-$10$\pm$10

magnetic field H is supplied by a superconducting coil, working in a nonpersistent mode. In order to prevent eddy currents, the experimental cell is entirely built out of epoxy resin Stycast 1266.[22]

During the measuring procedure, the sample is first zero-field cooled in the residual field of the cryostat ($H^{res}\simeq$10 mOe) from well above T_c and then stabilized at a fixed temperature T. Next, a magnetic field H applied perpendicularly to the ab planes is gradually increased from zero to H^{max} before being removed linearly at a rate of 9 T/s. This fast rate is achieved by shorting the superconducting coil ($L\simeq$7 H) over an extremely nonlinear resistor. Measurements of the current in the coil show that no discontinuities occur during the removal of the field. The data are taken as soon as the decreasing magnetic field fulfills the condition $H<1$ Oe. As a time origin for the measured data, we choose the time at which H starts being removed. After measuring the relaxation of the remanent magnetization M_{rem} for about seven time decades, the sample is heated above T_c in order to record its residual magnetization. The maximum values of the initially applied magnetic field H^{max} are shown in Table I for all the measuring temperatures T. The values of H^{max} are chosen so that they are bigger than twice the field needed to achieve full flux penetration into the sample. Table I further contains the values of the residual field H^{res} along the axis of the superconducting coil after cycling the magnetic field from zero to H^{max} and back to zero again.

Because of the high field removal rate $\dot{H}=9$ T/s, it was necessary to perform some controls concerning the initial field profile in the sample as well as self-heating effects. Several field removal rates $\dot{H}$ have been tested. We found that for the field removal rates 10^{-2} T/s$\leqslant\dot{H}\leqslant$9 T/s, the measured remanent magnetizations M_{rem} do not show any remarkable difference. Moreover, no significant change in the dynamics of the relaxation of M_{rem} could be detected by increasing the initial field values H^{max} by a factor of 2–3. From our estimations we concluded that the self-heating of the sample due to induction as well as to flux flow can be neglected for all temperatures and fields of our measurements.

With the described experimental procedure, there is only a small uncertainty of the time origin of the creep process ($<18\times10^{-3}$ s). The initial behavior of the relaxation data as a function of time is therefore very well defined so that we were able to test the existing vortex-creep models over a wide current density region starting from values near j_c.

III. FLUX DYNAMICS MODELS

The main effect of pinning is to allow a flux density gradient to be sustained within a type-II superconductor. This is intrinsically related to the flow of a macroscopic diamagnetic screening current density j that can be expressed, in the continuous approximation, through Maxwell's equation $\nabla\wedge\mathbf{B}=4\pi/c\,\mathbf{j}$. The configuration with a finite flux density gradient is metastable and hence is bound to decay. The dynamics arises from the vortex-creep motion as a result of thermal activation[23] and quantum tunneling[24,25] ($T\lesssim$5 K). For a geometry where $\mathbf{B}\|\hat{z}$ and $\mathbf{j}\|\hat{y}$, the Maxwell equations together with the condition of flux conservation lead to the nonlinear diffusion equation[26,27]

$$\frac{\partial j}{\partial t}=\frac{c}{4\pi}\frac{\partial^2}{\partial x^2}(vB). \tag{1}$$

Anderson[28] postulated that the velocity of the vortices, as a consequence of thermal activation over the pinning barrier $U(j)$, be given by

$$v=v_0(j)\exp\left(-\frac{U(j)}{k_BT}\right), \tag{2}$$

where $v_0(j)$ is the mean vortex velocity and can be expressed as $v_0(j)=l(j)/\tau_0$, where $l(j)$ is the mean hopping length and τ_0 is the inverse attempt frequency. For a situation where $v_0(j)$ is independent of j, the diffusion equation (1) can be transformed into

$$\frac{\partial j}{\partial t}\simeq-\frac{j_c}{\tau_0}\exp\left(-\frac{U(j)}{k_BT}\right). \tag{3}$$

As discussed by Geshkenbein and Larkin,[29] Eq. (3) can be solved within logarithmic accuracy, yielding

$$U(j(t))\simeq k_BT\,\ln\left(1+\frac{t}{t_0}\right), \tag{4}$$

where $t_0=k_BT\tau_0/j_c|\partial_jU|$ is a time scaling factor. Once the functional dependence between the pinning barrier U and the current density j is known, the time dependence of j is simply determined by the inversion of (4).

On approaching the critical current density j_c, the effective pinning barrier vanishes and one can write

$$U(j\rightarrow j_c)\simeq U_c\left(1-\frac{j}{j_c}\right)^{\alpha}. \tag{5}$$

Comparing Eqs. (4) and (5), the following time dependence of j is obtained:

$$j(t)\simeq j_c\left[1-\left\{\frac{k_BT}{U_c}\ln\left(1+\frac{t}{t_0}\right)\right\}^{1/\alpha}\right],\quad j\rightarrow j_c, \tag{6}$$

which maps to the original formulation of Anderson[28] for $\alpha=1$.

In the above derivation it is assumed that the current densities j are close to j_c. This is a good assumption for conventional type-II superconductors. Further theoretical considerations are necessary to describe the strongly decaying current densities in HTSC's, for which values of j much smaller than j_c are reached already at laboratory times. For the HTSC's in the limit of small currents, the weak collective pinning theory[13] (WCPT) and the vortex glass theory[14] predict an activation barrier that diverges algebraically for vanishing currents:

$$U(j)\simeq U_c\left(\frac{j_c}{j}\right)^{\mu}. \tag{7}$$

Inserting relation (7) into Eq. (4) the following nonpurely logarithmic time dependence of the current density j is obtained:

$$j(t)\simeq j_c\left[\frac{k_BT}{U_c}\ln\left(\frac{t}{t_0}\right)\right]^{-1/\mu}, \quad j\ll j_c. \tag{8}$$

In order to find a more general formula, (8) and (6) (we assume $\alpha=1$) can be interpolated with the expression

$$j(t)\simeq j_c\left[1+\mu\frac{k_BT}{U_c}\ln\left(1+\frac{t}{t_0}\right)\right]^{-1/\mu}, \tag{9}$$

and the corresponding activation barrier is [see Eq. (4)]

$$U(j)\simeq\frac{U_c}{\mu}\left[\left(\frac{j_c}{j}\right)^{\mu}-1\right]. \tag{10}$$

Within the *single-vortex* pinning regime, the exponent $1/\mu\approx 7$ is large, such that for $\mu k_BT/U_c\ln(1+t/t_0)\ll 1$ expression (9) can be approximated by

$$j(t)\simeq j_c\left(1+\frac{t}{t_0}\right)^{-k_BT/U_c}, \tag{11}$$

with a logarithmic potential

$$U(j)\simeq U_c\ln(j_c/j). \tag{12}$$

Notice that within the WCPT the divergence in the potentials (7), (10), and (12) at low current densities j is related to the observation that the activated motion of vortices involves hops of larger vortex segments or bundles over longer distances. The elastic energy cost will therefore grow with decreasing j. This is no longer the case for the pointlike pancake vortices for which no extra deformation energy is needed in order to overcome the pinning barrier for decreasing current densities. For strongly layered superconductors within the *single-pancake* creep regime, the activation barrier $U(j)$ is therefore expected to saturate. However, using the concept of variable-range hopping[30,31] (VRH) it has been argued[13] that, for decreasing current densities j, pancake vortices still couple into a two-dimensional (2D) elastic manifold. As a matter of fact, because of the randomness in the energies of the metastable state, pancakes will hop over larger distances as the current density j decreases. Such a large hopping distance u leads to a large shear interaction energy $c_{66}du^2$ between pancakes (c_{66} is the shear modulus and d the interlayer distance). As a consequence, for a large enough hopping distance u, the pancake vortex will start to couple to its neighbors. Thus the vortex system is expected to first go through a VRH regime, which is followed by a 2D collective creep regime[6] at still lower current densities.

In the above treatment of the flux dynamics models, we have considered current densities j flowing inside a superconductor, whereas from the experiment we obtain spatially averaged values of the magnetization M. In the case of an infinite slab parallel to the applied magnetic field H, the dependence between M and j has been described by Bean.[32] Recently, Gurevich and Brandt[33] obtained an asymptotic solution for the nonlinear diffusion equation (1) describing flux creep in strips and disks starting from a barrier as given in formula (10). It turns out that, despite the particular field distribution for these sample geometries, the current density j can still be considered as constant throughout the sample at a given time t. It follows that the magnetization M, which is given by

$$\mathbf{M}(t)=\frac{1}{V}\frac{1}{2c}\int \mathbf{r}\wedge\mathbf{j}(\mathbf{r},t)\,dV, \tag{13}$$

for a disklike geometry and for a constant current density $\mathbf{j}(\mathbf{r},t)=j(t)\mathbf{e}_{\phi}$, can be expressed as

$$|\mathbf{M}(t)|=j(t)\frac{1}{V}\frac{1}{2c}\int |\mathbf{r}\wedge\mathbf{e}_{\phi}|\,dV, \tag{14}$$

where the integration over the geometrical factor leads to

$$M(t)\simeq\frac{R}{3c}j(t), \tag{15}$$

with R being the sample radius. For the case of disks (strips) the well-known Bean model relationship for an infinite cylinder (infinite slab) in the fully critical state is therefore still a valid approximation.

IV. VORTICES IN STRONGLY LAYERED SUPERCONDUCTORS

For the considerations given in this section concerning the vortex lattice in coupled superconducting layers, we will closely follow the approach of Refs. 13 and 34. Within weak collective pinning theory the size of the correlated regions (Larkin domains) is determined by the balance between deformation energy and pinning energy. In terms of length scales, the volume forming the Larkin domain is given by the pinning correlation lengths R_c and L_c in the direction perpendicular and parallel to the magnetic field, respectively. Through the study of the relative magnitude of the deformation and the pinning energy of a vortex lattice in coupled superconducting layers, it is possible to determine the size of the correlated regions as a function of temperature and field.

For a magnetic field H perpendicular to the superconducting layers, a vortex lattice has three relevant energy scales, namely, the tilt energy $U_{\rm tilt}\approx c_{44}(R_c)\cdot[(r_p/L_c)^2R_c^2L_c]$, the shear energy $U_{\rm shear}\approx c_{66}\cdot[(r_p/R_c)^2R_c^2L_c]$, and the pinning energy $U_{\rm pin}\approx(\gamma\xi^4R_c^2L_c/r_p^2a_0^2)^{1/2}$, with c_{44} being the dispersive tilt modulus, c_{66} the shear modulus, $r_p(T)$ the range of the pinning force, a_0 the intervortex spacing, and γ the dis-

order strength [where a short-scale correlated disorder potential has been assumed $\langle U_{\rm pin}(r), U_{\rm pin}(r')\rangle = \gamma\delta(r-r')$]. Depending on the relative magnitude of these energies, one can distinguish four possible pinning regimes: (1) independently pinned vortex pancakes (0D pinning regime, $U_{\rm pin} > U_{\rm tilt}$, $U_{\rm shear}$), (2) independently pinned vortex lines (1D pinning regime, $U_{\rm tilt} > U_{\rm pin} > U_{\rm shear}$), (3) a 2D collectively pinned state in which the 2D vortex lattices in the layers are pinned independently from each other ($U_{\rm shear} > U_{\rm pin} > U_{\rm tilt}$), and (4) a 3D collectively pinned state ($U_{\rm tilt}, U_{\rm shear} > U_{\rm pin}$).

According to Refs. 13 and 16, for temperatures $T < T_0 \approx (U_{\rm pc}^2 E_{\rm pc})^{1/3}$ and fields $B < B_{02} \approx 10\Phi_0/(2\pi\xi^2)$ $[j_c(0)/j_0]$, where T_0 is a few tens of kelvins and B_{02} is a few teslas, the dominant energy scale for strongly anisotropic Bi2212 is the pinning energy $U_{\rm pin}$ [where $U_{\rm pc} \simeq \varepsilon_0 d(j_c/j_0)$, $E_{\rm pc} \approx \varepsilon_0 d(\xi/\lambda)^2$, $\varepsilon_0 = (\Phi_0/4\pi\lambda)^2$, $\Phi_0 = hc/2e$, d is the interlayer distance, and j_0 the depairing current density]. The B-T phase diagram for this region is therefore characterized by 0D pinning. On the other hand, for temperatures $T > T_0$ the collective pinning length L_c and the collective pinning radius R_c both grow very fast as a result of thermal depinning. This implies that for temperatures $T \gtrsim 20$ K the size of the Larkin domains becomes large, giving rise to a 3D pinning regime.[16] At high fields $B > B_{23}$, a crossover to a 2D collective pinning region is predicted[13] when the shear energy outweighs the tilt energy.

Finally, since the relaxation measurements of the remanent magnetization $M_{\rm rem}$ presented in this work are performed in the "field-off" state, we need to discuss the very-low-field regime. At fields $B > \Phi_0/\lambda^2$, the shear modulus c_{66} has a linear dependence in B, whereas at low fields ($B < \Phi_0/\lambda^2$), c_{66} decreases exponentially,[16,35]

$$c_{66} \approx \begin{cases} \dfrac{\varepsilon_0}{\lambda^2}\left(\dfrac{B\lambda^2}{\Phi_0}\right)^{1/4} e^{-\sqrt{\Phi_0/B\lambda^2}}, & B < \Phi_0/\lambda^2, \\ \dfrac{\varepsilon_0 B}{4\Phi_0}, & B > \Phi_0/\lambda^2, \end{cases} \tag{16}$$

where λ is the penetration depth. As a consequence, also the shear energy $U_{\rm shear}$ decreases exponentially for fields $B < \phi_0/\lambda^2$. This means that for temperatures $T > T_0$ and small enough magnetic fields ($B < B_{13}$) a 1D pinning regime occurs. Figure 1 shows a qualitative map of the low-field pinning regimes of Bi2212 resulting from these considerations.

V. EXPERIMENTAL RESULTS AND ANALYSIS

In Fig. 2 we illustrate the time dependence of the remanent magnetization $M_{\rm rem}$ with a typical set of data. A nonlogarithmic behavior[20] is observed at all temperatures. Notice that at 25 K, where a sharp drop in the relaxation rate $S = -\partial \ln M_{\rm rem}/\partial \ln t$ has been previously reported,[17–19] the remanent magnetization $M_{\rm rem}$ decays extremely fast in the first few seconds after the removal of the external field H. This is also seen in Fig. 3, where the current density j [as obtained from formula (15)] is plotted as a function of temperature for the times $t_s \simeq 18\times10^{-3}$ s, $t_1 = 1$ s, and $t_2 = 10^4$ s. The data taken at the starting time $t_s \simeq 18\times10^{-3}$ s (open circles) suggest the presence of only two regimes of vortex dynamics, separated by a crossover at $T \simeq 30$ K. Both regimes are accurately described by an exponential temperature dependence, but with different slopes $d\ln j/dT$. However, at longer times $t \gtrsim 1$ s (solid circles and open diamonds), the existence of a third regime for temperatures between 20 and 40 K becomes evident. This third regime is characterized by very particular vortex dynamics and will be referred to as the "intermediate regime." We will discuss these temperature regimes separately and distinguish them as follows: a low-temperature regime for $T \lesssim 20$ K, an interme-

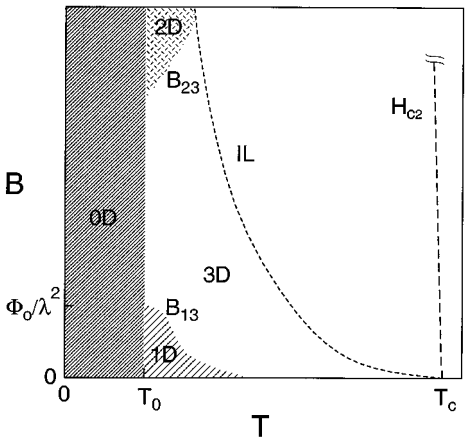

FIG. 1. Qualitative low-field phase diagram of the vortex state in Bi2212 for magnetic fields H perpendicular to the superconducting layers. The differently shaded areas in the figure represent the following pinning regimes: 0D, individually pinned pancake vortices; 1D, individually pinned vortex lines; 2D, collectively pinned state in which 2D lattices of pancake vortices in the layers are pinned independently from each other; 3D, collectively pinned vortex bundles. B_{13} (B_{23}) represents the fields at which the 1D (2D) regime crosses over to the 3D regime. T_0 is a crossover temperature terminating single-pancake pinning. A sketch of the irreversibility line IL and of the upper critical field H_{c2} is also given.

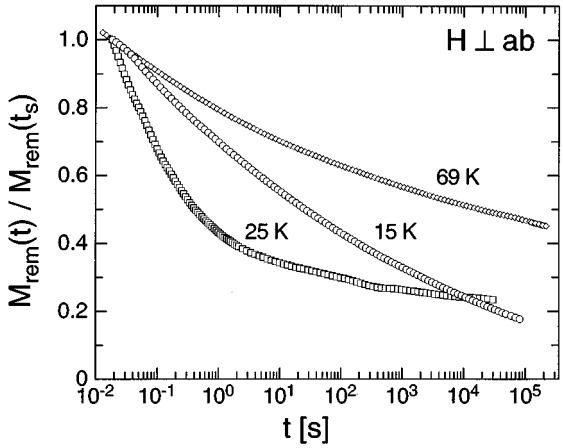

FIG. 2. Normalized remanent magnetization vs time, measured after cycling the sample in an external magnetic field H. In parentheses the values of the maximal cycling fields $H^{\rm max}$ are given: ○ ($H^{\rm max} = 1$ kOe) at 15 K, □ ($H^{\rm max} = 1$ kOe) at 25 K, and ◇ ($H^{\rm max} = 40$ Oe) at 69 K. The time origin is given by the instant when the externally applied magnetic field H starts being decreased, and $t_s \simeq 18\times10^{-3}$ s is the time when the first point of the relaxation of $M_{\rm rem}$ is taken.

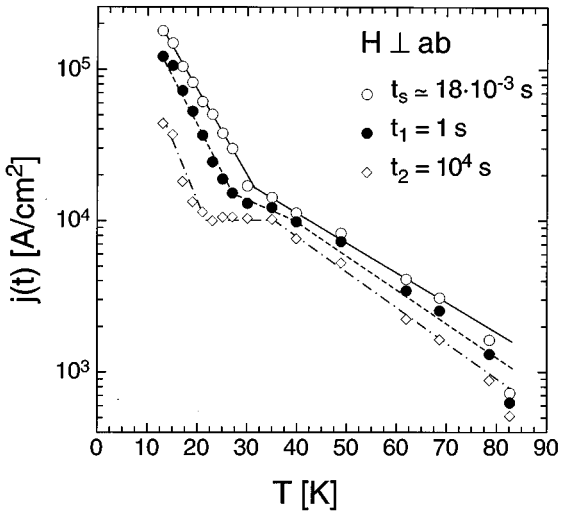

FIG. 3. Current density j as a function of temperature for different times t: ○ starting time $t_s \simeq 18\times10^{-3}$ s, ● $t_1=1$ s, and ◇ $t_2=10^4$ s. The lines serve as guides to the eyes.

diate regime for 20 K$\lesssim T \lesssim$40 K, and a high-temperature regime for $T \gtrsim 40$ K. For each regime we determine the activation barrier $U(j)$ by means of the method of Maley *et al.*[15] Once the functional dependence of $U(j)$ is obtained, an analysis of the time evolution of the current density j is given.

A. Low-temperature regime ($T \lesssim 20$ K)

As shown by Maley *et al.*, it is possible to determine the activation barrier for vortex motion $U(j)$ directly from the relaxation data $j(t)$. Starting from Eq. (3), one obtains

$$U(j) \simeq -k_B T \ln\left|s\frac{\partial j}{\partial t}\right| + k_B T \ln\left|s\frac{j_c}{\tau_0}\right|, \tag{17}$$

where the term $k_B T \ln|s j_c/\tau_0|$ is independent of j and $s=1$ cm^2 s/A. Plotting the expression $-k_B T \ln|s\partial j/\partial t|$ as a function of current density at different temperatures T, a set of curves is found which are vertically shifted with respect to each other. For a temperature interval where the functional dependence between the activation barrier U and the current density j is essentially temperature independent, this shift is given by the term $a\Delta T$, where $a \simeq \ln|s j_c/\tau_0|$ is a constant and $\Delta T = T_2 - T_1$ is the temperature difference between two considered curves. Combining the data measured at different temperatures T, the activation barrier $U(j)$ is obtained over a wide current density range.

For temperatures $T \lesssim 20$ K, the data obtained from the expression $-k_B T \ln|s\partial j/\partial t|$ at different temperatures T can be accurately mapped onto a common curve using a single constant a. The obtained potential $U(j)$ is shown in Fig. 4. It is interesting to observe in Fig. 4(a) that the data measured at a fixed temperature T (marked by horizontal segments) do overlap over wide regions of current. As seen in Fig. 4(b), the potential $U(j)$ is proportional to the logarithm of the current density j over a wide current region. This is in good agreement with previous relaxation measurements by van der Beek *et al.*[6] and by Emmen *et al.*,[7] who found a logarithmic dependence of $U(j)$ for temperatures 4K$\lesssim T \lesssim$17 K. The deviation from the logarithmic behavior at temperatures $T>19$ K is attributed to the influence of the approaching intermediate regime.

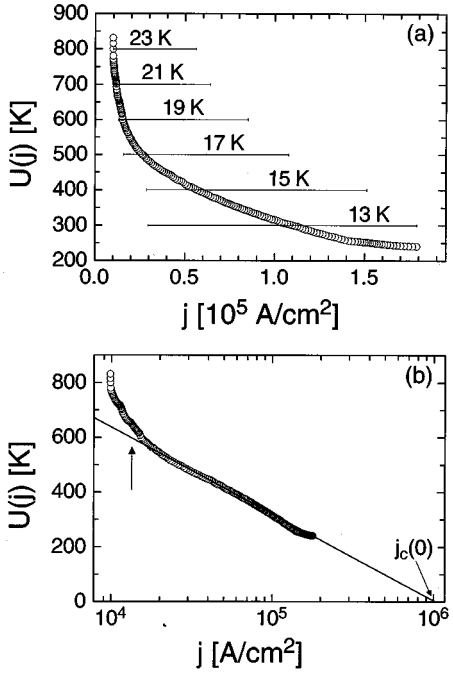

FIG. 4. (a) Flux-creep activation barrier for temperatures 13 K$\lesssim T \lesssim$23 K as determined from the magnetic relaxation data by the method of Maley *et al.* (the constant used for matching the curves is $a=26\pm1$). The horizontal segments represent the current windows as obtained from the data at a fixed temperature T. (b) The same data in a semilogarithmic graph. The line is a fit for temperatures up to $T=19$ K (indicated by the arrow) with a logarithmic potential of the type $U(j) \simeq U_c \ln(j_c/j)$. From the fit one finds the $T=0$ critical current density $j_c(0) \simeq (1.0\pm0.3)\times10^6$ A/cm^2.

For temperatures $T \lesssim 19$ K, a fit to the measured potential $U(j)$ with the logarithmic activation barrier (12) leads to the following parameters: $U_c \simeq 140$ K and the extrapolated critical current density $j_c(T=0) \simeq 1\times10^6$ A/cm^2. The value of $j_c(T=0)$ is very close to the values found in the literature[6,7] (taking into account the considered proportionality factors between M and j).

As discussed in Sec. III, the activation barrier $U(j)$ is expected to be logarithmic within the single-vortex pinning regime. Since the measured potential $U(j)$ is indeed logarithmic, this would suggest that for temperatures $T \lesssim 20$ K vortex strings are pinned individually. However, a simple estimate of the collective pinning length along the c axis, $L_c^c \simeq \varepsilon\xi(j_0/j_c)^{1/2}$, where ε is the anisotropy factor and j_0 is the depairing current density, shows that, for the parameters of Tables II and III, $L_c^c \simeq 2$ Å$<d=15$ Å. This means that, for temperatures $T \lesssim 20$ K and low enough magnetic fields, pancake vortices placed on different superconducting layers are pinned independently, indicating the presence of a single-pancake pinning regime. A more detailed discussion of the low-temperature activation barrier will be given in Sec. VI.

We can crosscheck the result for the barrier as obtained via the Maley analysis making use of Eqs. (11) and (15). A typical fit to the data measured at temperatures $T \lesssim 19$ K is shown in Fig. 5, confirming the logarithmic dependence

TABLE II. Experimental fitting parameters obtained from the relaxation data in the low-temperature regime ($T \lesssim 20$ K) and in the high-temperature regime ($T \gtrsim 40$ K).

	U_c (K)	t_0 (s)	$j_c(T=0)$ (A/cm^2)	μ
$T \lesssim 20$ (K)	140	3×10^{-2}	1×10^{6}	0
$T \gtrsim 40$ (K)	1000	3×10^{-3}		0.6

$U(j) \simeq U_c \ln(j_c/j)$. The resulting fitting parameters are the following: $U_c \simeq 140$ K, $t_0 \simeq 3\times10^{-2}$ s, and values of $j_c(T)$ about 5% above the values shown in Fig. 3 for $t_s \simeq 18 \times 10^{-3}$ s.

Finally, we point out that for temperatures $T \lesssim 20$ K the values of the pinning potential $U(j)$ and of the extrapolated critical current density $j_c(T=0)$ are both in good agreement with the results in the literature, usually obtained in the field-on mode at much slower field ramping rates $\dot{H}$.

B. Intermediate regime (20 K$\lesssim T \lesssim$40 K)

In order to find the activation barrier $U(j)$ for temperatures 20 K$\lesssim T \lesssim$40 K, the relaxation data are again evaluated with the method of Maley *et al.* The results obtained with help of Eq. (17) for different temperatures T are shown in Fig. 6. We observe that the curves are strongly tilted with respect to each other, and it is not possible to obtain a unique smooth curve by simply shifting the data obtained at different temperatures T along the vertical axis. Thus, within the temperature range 20 K$\lesssim T \lesssim$40 K, we cannot find a unique temperature-independent functional relation between U and j following the above approach. A qualitative interpretation of the vortex dynamics in this temperature regime will be given in Sec. VI.

C. High-temperature regime (40 K$\lesssim T \lesssim$83 K)

For temperatures $T \gtrsim 40$ K, the activation barrier $U(j)$ is found with the same method that has been applied for the low-temperature regime using a single constant a. The resulting barrier $U(j)$ is shown in Fig. 7. From the double logarithmic plot of Fig. 7(b), we observe that the activation barrier $U(j)$ follows a power-law behavior over a wide current range. Fitting this potential with formula (10) for temperatures 62 K$\lesssim T \lesssim$83 K, we find the values $U_c \simeq 1000$ K and $\mu \simeq 0.6$.

According to Ref. 13, a power-law potential with the form of (10) leads to a time dependence of the current density j as given by the interpolation formula (9). As one can see from the solid line of the fit to the $T=69$ K data in Fig. 5, the time dependence of the current density j is very well described by the interpolation formula (9). The fitting parameters confirm the results previously obtained for the barrier and can be summarized as follows (see also Table II: $U_c \simeq 1000$ K, $\mu \simeq 0.6$, $t_0 \simeq 3\times10^{-3}$ s, and values of $j_c(T)$ about 5% above those obtained from Fig. 3 at $t_s \simeq 18\times10^{-3}$ s. According to weak collective pinning theory, an exponent $\mu \simeq 0.6$ indicates a regime of large 3D bundle pinning.

TABLE III. Values of j_0, $j_0/j_c(0)$, $L_c^c(0)$, $E_{\rm pc}$, and $U_{\rm pc}$ as obtained from the following formulas: $j_0 = c\Phi_0/(12\sqrt{3}\pi^2\lambda^2\xi)$, $L_c^c \simeq \varepsilon\xi(j_0/j_c)^{1/2}$, $E_{\rm pc} \approx \varepsilon_0 d(\xi/\lambda)^2$, and $U_{\rm pc} \simeq \varepsilon_0 d(j_c/j_0)$. The parameters used for the theoretical estimates are given for the configuration where H is perpendicular to the superconducting layers.

$j_0 \approx 10^8$ (A/cm^2)	$U_{\rm pc} \simeq 20$ (K)	
$j_0/j_c(0) \approx 100$	$E_{\rm pc} \approx 3\times10^{-2}$ (K)	$L_c^c(0) \simeq 2$ (Å)
$\lambda_L \simeq 1800$ (Å)	$\lambda(0) = \lambda_L/\sqrt{2} \simeq 1300$ (Å)	$d \simeq 15$ (Å)
$\xi_{\rm BCS} \simeq 30$ (Å)	$\xi(0) = \sqrt{0.54}\xi_{\rm BCS} \simeq 20$ (Å)	$\varepsilon \simeq 1/150$

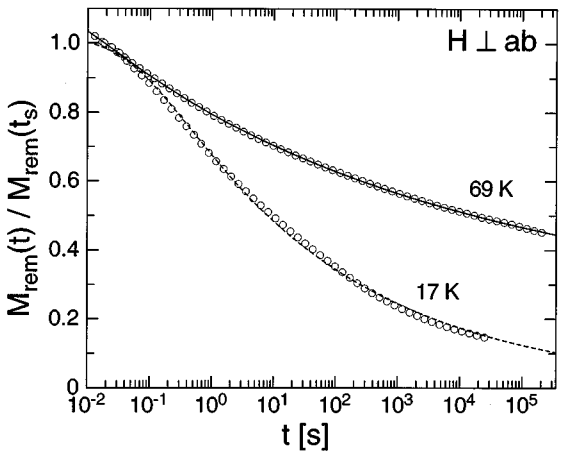

FIG. 5. Normalized remanent magnetization vs time for temperatures $T=17$ and 69 K. The lines are fits according to formula (11) for the 17-K data and formula (9) for the 69-K data.

The high-temperature data have been analyzed considering a constant current density j inside the sample as assumed in the Bean model [see formula (15)]. We argue that, for the present measurements of the relaxation of the remanent magnetization $M_{\rm rem}$, the contributions of pinning due to potential barriers arising from surface effects[36–39] and sample geometry[40,41] have only a secondary effect as compared to the contributions of bulk pinning. As a matter of fact, if surface barriers were the only mechanism responsible for the irreversible behavior, the magnetization curves would be characterized by *zero magnetization* on the descending

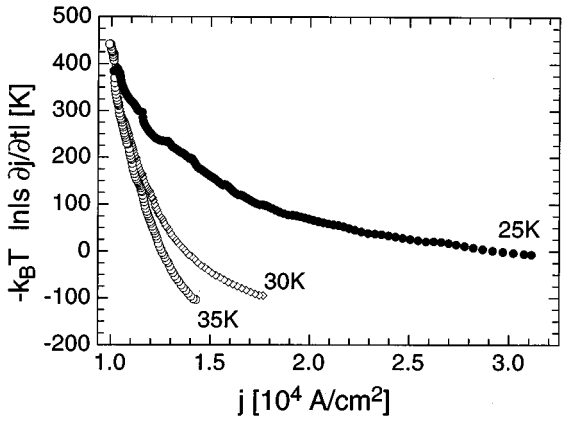

FIG. 6. Flux-creep activation barrier vs current density j for temperatures 23 K$\lesssim T \lesssim$35 K. The vertical axis is only defined up to a constant value. For this temperature regime the curves are strongly tilted with respect to each other and cannot be "glued" onto a common curve anymore.

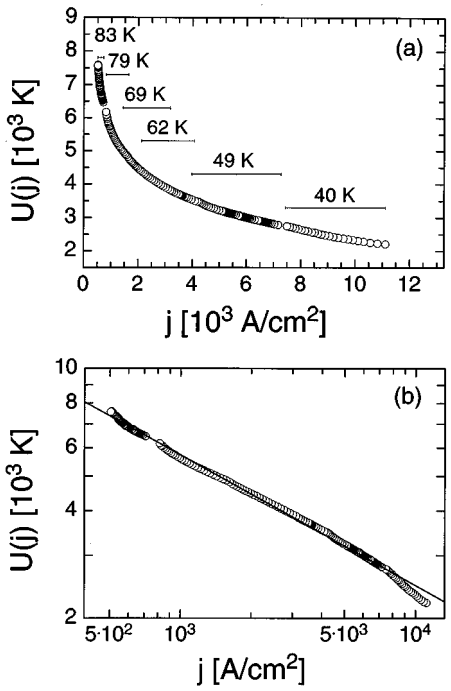

FIG. 7. (a) Flux-creep activation barrier for 40 K$\leqslant T\leqslant$83 K as determined by the method of Maley *et al.* (with $a=62\pm1$) from the magnetic relaxation data. The horizontal segments represent the current windows as obtained from the data at a fixed temperature T. (b) The same data in a double-logarithmic graph. The line is a fit for temperatures $T\geqslant$62 K, with a power-law potential as given in formula (10).

branch of the loop.[37–39] Figure 8 shows three magnetization cycles of the Bi2212 crystal measured at different temperatures T. From the shape of the curves, we can safely say that, for our sample, pinning due to surface barriers does not play a dominant role. In thin superconducting strips of rectangular cross section, Meissner currents flow throughout the whole sample[42,43] and not only in a surface layer of width λ. Lor-

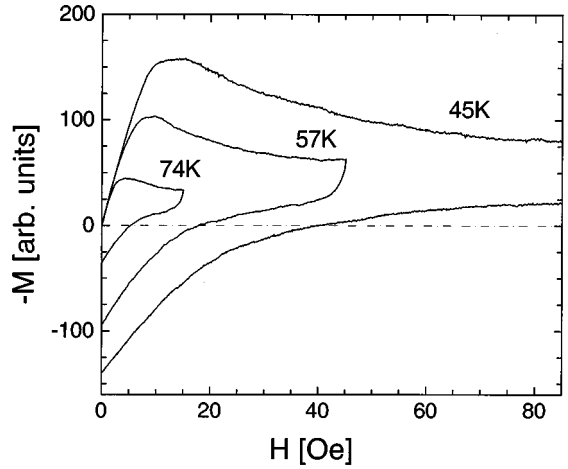

FIG. 8. Magnetization curves at different temperatures T for the Bi2212 crystal. The descending branches of the loops do not have zero magnetization so that we conclude that Bean-Livingston surface barriers are only of secondary importance.

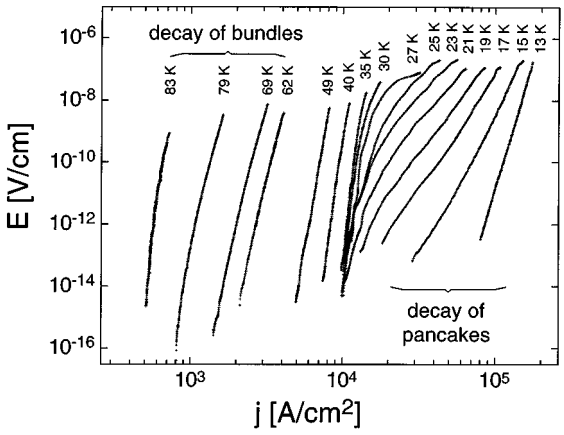

FIG. 9. Current-voltage characteristics as extracted from the relaxation data for different temperatures T at zero external field H.

entz forces arising from the Meissner currents will therefore act on the vortices and give rise to a barrier of purely geometric origin.[40] This kind of geometrical barrier will *not* influence measurements performed in the field-off state, since Meissner currents do not flow in this state (the influence of the residual fields $H^{\rm res}$ is of minor importance; see Table I).

D. Current-voltage characteristics

Inductive measurements of the relaxation of the remanent magnetization $M_{\rm rem}$ are a powerful tool[8,44,45] for the evaluation of $E(j)$ characteristics of a superconductor down to *very* low values of the electric field E. The functional dependence between the electric field E and the current density j can be found as follows. In the Coulomb gauge $\nabla\cdot\mathbf{A}=0$, the vector potential $\mathbf{A}$ can be expressed as

$$\mathbf{A}(\mathbf{r})=\frac{1}{c}\int\frac{\mathbf{j}(\mathbf{r}')}{|\mathbf{r}-\mathbf{r}'|}d^3r', \tag{18}$$

where $\mathbf{j}$ is the current density. For a disklike geometry and for a constant current density $\mathbf{j}(\mathbf{r}')=j\mathbf{e}_\phi$ ($j=$const), one obtains

$$|\mathbf{A}(\mathbf{r})|\simeq j\frac{1}{c}\int_V\frac{d^3r'}{|\mathbf{r}-\mathbf{r}'|}, \tag{19}$$

which, together with the Faraday induction law $\partial_t\mathbf{A}=-c\mathbf{E}$, leads to

$$E=\frac{\gamma}{c^2}hR\frac{\partial j}{\partial t},\quad \gamma\simeq2, \tag{20}$$

where E is the mean electrical field in the sample, R the sample radius, and h its thickness. The constant factor γ arises from the assumption of a disklike geometry for the sample.

The results obtained from the magnetic relaxation data and Eq. (20) are plotted in Fig. 9. From the graph one can clearly distinguish the three regimes of vortex dynamics, which were previously discussed in this section. For current densities $j \lesssim j_c$, the electric field E due to the dissipative process of thermally activated vortex drift can be written as[33]

$$E(j) = E_c \exp[-U(j)/k_B T]. \tag{21}$$

From Fig. 9 it is seen that for temperatures $T \lesssim 19$ K the $E(j)$ curves follow a power-law behavior. As a matter of fact, inserting the logarithmic potential (12) into formula (21) one obtains

$$\frac{E}{E_c} = \left(\frac{j}{j_c}\right)^{U_c/k_B T}. \tag{22}$$

From a fit to the curves in this temperature regime, we obtain again $U_c \simeq 140$ K, in agreement with the previous results.

For temperatures 20 K$\lesssim T \lesssim$35 K, the electric field $E(j)$ behaves like a power law only at high current densities. For smaller values of the current density j, the different $E(j)$ curves tend to converge into the $T=35$ K curve. Further details about this temperature regime will be given in the next section.

Finally, for temperatures $T \gtrsim 60$ K, the $E(j)$ curves have a *negative* curvature in the log$E$-log$j$ plot, in agreement with the interpolation formula (10) for the barrier as obtained from WCPT. The fitting parameter $U_c \approx 1000$ K is again consistent with our previous results.

VI. SUMMARY AND DISCUSSION

The results obtained in the previous section for the strongly layered Bi2212 single crystal in magnetic fields $\mathbf{H} \perp ab$ planes are now summarized and further discussed within the frame of WCPT.

For temperatures $T \lesssim 20$ K, the activation barrier for vortex motion $U(j)$ depends logarithmically on the current density, while the time relaxation of the current density j follows a power-law behavior as given by formula (11). According to the discussion in Sec. III, an approximately logarithmic current dependence in the activation barrier (12) is obtained within the single-vortex pinning situation. However, in Sec. V it has been shown that for temperatures $T \lesssim 20$ K and small enough magnetic fields the correlation length along the c axis, L_c^c, is much smaller than the interlayer distance d. This indicates that for this regime pinning involves elementary pancake vortices.

On the other hand, within the most simple approach (see Sec. III), for decreasing current densities j the activation barrier for single pancakes $U(j)$ is expected to be a constant, whereas the measured activation barrier is found to be logarithmic up to temperatures $T \simeq 19$ K. The nonconstant behavior of the measured activation barrier $U(j)$ suggests that there are residual interactions which were not considered in the most simple approach and which lead to an increase of the elastic energy for decreasing j. This argument is also supported by the following considerations: The collective pinning energy for single pancakes,[13] which is the relevant parameter for the determination of quantities such as the critical current density j_c and the depinning energy, is given by $U_{\rm pc} \simeq \varepsilon_0 d(j_c/j_0)$. For the parameters of Tables II and III one finds that $U_{\rm pc} \simeq 20$ K. Furthermore, the energy which is relevant for creep of pancake vortices is expected to be bigger than $U_{\rm pc}$, but of the same order of magnitude. However, this estimated energy is still small as compared to the values obtained for the activation energy $U(j)$ plotted in Fig. 4, indicating that for creep of pancake vortices additional interactions have to be considered. A possible idea leading to coupling of the pancake vortices into an elastic plane[13] for decreasing current densities j is the concept of variable-range hopping. As discussed in Sec. III, because of the randomness in the energies of the metastable state, pancakes will hop over larger distances as the current density j decreases. The shear interaction energy $c_{66} d u^2$ will therefore grow with increasing hopping distance u and for low enough current densities $c_{66} d u^2$ will become of the order of the pinning energy $U_{\rm pc}$. In summary, the vortex system is expected to go over from a VRH regime (creep of individual pancake vortices) to a 2D collective creep regime at low current densities.

At higher temperatures ($T \gtrsim 20$ K), where bulk pinning becomes relatively weak, barriers arising from the geometry of the sample and from surface effects can play an important role. As shown in Sec. V, in the low magnetic induction regime (field-off creep measurements) and for our specimen, these contributions are of minor importance as compared to the contributions of bulk pinning.

For temperatures $T \gtrsim 40$ K, the activation barrier $U(j)$ is found to follow a power-law behavior (Fig. 7) that can be accurately fitted with formula (10). Within WCPT it has been shown that a potential of the form of (10) leads to a time relaxation of the current density j as given by the interpolation formula (9). From the fit to the $T=69$ K data in Fig. 5, it is seen that for this temperature regime the time dependence of the current density j is actually well described by formula (9). According to WCPT, a power-law potential with an exponent $\mu \simeq 0.6$, as obtained from the fits, indicates a regime of large bundle pinning. A list of the obtained fitting parameters is given in Table II.

No unique functional dependence between U and j could be found for the temperature range 20 K$\lesssim T \lesssim$40 K. Motivated by the present experimental results, the very-low-field regime of the Bi2212 pinning diagram has been investigated. Figure 1 shows the qualitative diagram obtained for this regime. For temperatures T above T_0, two different pinning regimes separated by B_{13} are found involving vortex pancakes and vortex segments. In order to describe the relaxation data in this temperature regime, it is therefore necessary to estimate the induction in the center of the sample ($B_{\rm center}$) at the time $t = t_s \simeq 18 \times 10^{-3}$ s, immediately after removing the external field H. These values are given for all temperatures by the open circles in Fig. 10, where the arrows indicate the time evolution of $B_{\rm center}$ during the relaxation of the remanent magnetization $M_{\rm rem}$. For temperatures $T \lesssim 20$ K and $T \gtrsim 40$ K, it follows that the whole sample is characterized by 0D and 3D pinning, respectively. On the other hand,

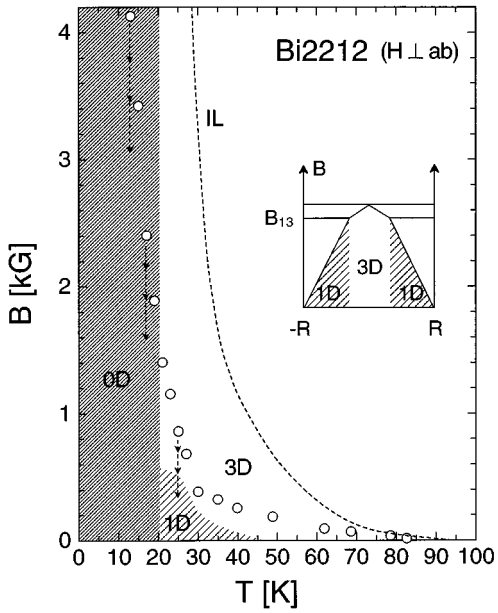

FIG. 10. Qualitative low-field phase diagram of the vortex state in Bi2212 as proposed in Fig. 1 (the 2D regime is not shown in this plot since it is not relevant for the present data range). The open circles in the graph are the estimated values of the B field at the center of the sample (B_{center}) at the starting time $t=t_s\simeq 18\times 10^{-3}$ s, just after removing the external field H. The vertical arrows qualitatively show the time evolution of B_{center} during the relaxation of the remanent magnetization M_{rem}. The inset represents schematically the profiles of the induction B in the remanent state for temperatures between 20 and 40 K. The shaded areas indicate the different pinning regimes throughout the sample (here R is the sample radius). In particular, the parameter B_{13} in the inset indicates the value of the induction B in the sample at which 1D pinning goes over into 3D pinning. The smoothed irreversibility line IL in the graph was obtained from the data of Schilling *et al.* (Ref. 46).

as shown in the inset of Fig. 10, for temperatures 20 K$\lesssim T\lesssim$40 K, the values of the initial field profile in the sample lead to the *coexistence* of two different pinning regimes: 3D pinning in the central region of the sample and 1D pinning close to the borders. The simultaneous occurrence of two different pinning regimes may then provide an explanation why no simple functional dependence between U and j could be found for this temperature interval.

From the analysis of the relaxation data, we find that vortex bundles are strongly pinned against thermal activation. Nevertheless, because of their large size, they can only sustain low flux density gradients, which means low critical current densities j_c. On the other hand, vortex strings are weakly pinned, but being small in size they can sustain relatively high flux density gradients. Much higher creep rates are therefore expected for collectively pinned vortex lines than for large vortex bundles. Thus a possible interpretation of the vortex dynamics observed for the temperature interval 20 K$\lesssim T\lesssim$40 K is the following: The high relaxation rates which are measured at times $t\lesssim 1$ s (see Fig. 2) are mainly the result of the strong decay of the flux in the 1D regime at the border areas of the sample. At times $t\gtrsim 1$ s, most of the flux has left the sample and only a low flux density gradient of vortex strings remains. As discussed in Sec. III, at low current densities j the activated motion of vortex lines involves hops of larger vortex segments by longer distances. The weak relaxation rates of the current density j measured at times $t\gtrsim 1$ s are then explained by the growth of the elastic energy for the activated motion of vortex strings at low current densities.

A feature that has recently attracted a lot of interest in the literature is the observation of a second peak in the magnetization loop.[47] In our Bi2212 sample, as well as in several other works on Bi2212,[41,48–51] this second peak is seen for magnetic inductions B of the order of Φ_0/λ^2 and for temperatures between 20 and 40 K. As discussed in Sec. IV, for magnetic inductions $B\lesssim\Phi_0/\lambda^2$ the shear modulus c_{66} starts to decrease exponentially so that, at low fields and for temperatures $T\gtrsim$20 K, a 1D pinning regime can arise (see Fig. 1). For the ascending branch of a magnetization loop, it follows that, for fields larger than the field of first flux penetration H_p, the sample is expected to first enter into the 1D regime before gradually going over into 3D. As previously discussed, at a fixed temperature T, the value of j_c is bigger for the 1D regime than for the 3D regime. However, since the flux in the 1D regime has a much faster creep rate as compared to the 3D regime, it is very important to consider the *time scale* for the measurement of the magnetization loop. For instance, if the time scale were very short ($t\to 0$), the effects of creep would be negligible and for an increasing (decreasing) magnetic field H one would expect to measure a *decrease* (*increase*) in the magnetization as soon as the magnetic induction B is of the order of Φ_0/λ^2, where the flux in the sample goes over from 1D to 3D. On the other hand, on the typical time scale of the measurement of a magnetization loop, the flux in the 1D regime is already strongly relaxed, while the flux in the 3D regime is still close to its configuration in the critical state. The value of the magnetization M may then turn out to be smaller in the 1D regime than in the 3D regime, leading to the characteristic double peak in the magnetization loop as measured for temperatures between 20 and 40 K.

This interpretation is in agreement with previous reports[51–53] which relate the second peak of the magnetization loop to the slower magnetization decay for the field range where the peak is observed. Moreover, it is in agreement with the results of Ref. 41 regarding local induction measurements on a Bi2212 sample. In the descending branch of the magnetization loop, at $T=24$ K and for field values between 330 and 260 Oe, a change of slope of the field profile $dB_z(x)/dx$ is observed[41] occurring at various locations inside the crystal starting from the edge regions and moving towards the center as the applied field is decreased (with B_z being the induction parallel to the crystallographic c axis). Within the presented low-field phase diagram of Bi2212, this change of slope is expected to occur at the crossover field B_{13}.

In conclusion, for temperatures 20 K$\lesssim T\lesssim$40 K, the observation of the second peak in the magnetization loop and of the high relaxation rates of the current density j for times $t\lesssim 1$ s can both be related to the coexistence of two different pinning regimes inside the sample and to the strong difference in their relaxation rates.

ACKNOWLEDGMENTS

It is a pleasure to acknowledge many helpful discussions with V. B. Geshkenbein, C. de Morais-Smith, T. Teruzzi, K. Aupke, R. Frassanito, M. Kugler, and A. Amann. We are grateful to V. N. Zavaritzky for providing the Bi2212 sample. A.S. would like to thank D. Brinkmann for his kind support. This work was supported by the Schweizerischer Nationalfonds zur Förderung der wissenschaftlichen Forschung and by the Eidgenössische Stiftung zur Förderung der schweizerischen Volkswirtschaft durch wissenschaftliche Forschung.

---

*Present address: Physik-Institut der Universität Zürich, Winterthurerstr. 190, 8057 Zürich, Switzerland.

[1] J. R. Clem, Phys. Rev. B **43**, 7837 (1991).
[2] H. Safar, C. Durán, J. Guimpel, L. Civale, J. Luzuriaga, E. Rodriguez, F. de la Cruz, C. Fainstein, L. F. Schneemeyer, and J. V. Waszczak, Phys. Rev. B **40**, 7380 (1989).
[3] P. Svendlindh, C. Rossel, K. Niskanen, P. Norling, P. Nordblad, L. Lundgren, and G. V. Chandrasekhar, Physica C **176**, 336 (1991).
[4] D. Shi and M. Xu, Phys. Rev. B **44**, 4548 (1991).
[5] D. Hu, W. Paul, and J. Rhyner, Physica C **200**, 359 (1992).
[6] C. J. van der Beek, P. H. Kes, M. P. Maley, M. J. V. Menken, and A. A. Menovsky, Physica C **195**, 307 (1992).
[7] J. H. P. M. Emmen, V. A. M. Brabers, and W. J. M. de Jonge, J. Alloys Compounds **195**, 439 (1993).
[8] A. A. Zhukov, H. Kupfer, V. A. Rybachuk, L. A. Ponomarenko, V. A. Murahov, and A. Yu. Martynkin, Physica C **219**, 99 (1994).
[9] J. G. Bednorz and K. A. Müller, Z. Phys. **64**, 189 (1986).
[10] H. Küpfer, C. Keller, R. Meier-Hirmer, U. Wiech, K. Salama, V. Selvamanickam, S. M. Green, H. L. Luo, and C. Politis, Phys. Rev. B **41**, 838 (1990).
[11] L. Gao, Y. Y. Xue, P. H. Hor, and C. W. Chu, Physica C **177**, 438 (1991).
[12] T. Puig, P. G. Huggard, M. Pont, Gi. Schneider, J. S. Muñoz, and W. Prettl, Phys. Rev. B **49**, 7004 (1994).
[13] A. I. Larkin and Yu. N. Ovchinnikov, J. Low Temp. Phys. **34**, 409 (1979); V. M. Vinokur, M. V. Feigel'man, V. B. Geshkenbein, and A. I. Larkin, Phys. Rev. Lett. **65**, 259 (1990); G. Blatter, M. V. Feigel'man, V. B. Geshkenbein, A. I. Larkin, and V. M. Vinokur, Rev. Mod. Phys. **66**, 1125 (1994).
[14] M. P. A. Fisher, Phys. Rev. Lett. **62**, 1415 (1989); D. S. Fisher, M. P. A. Fisher, and D. A. Huse, Phys. Rev. B **43**, 130 (1991).
[15] M. P. Maley, J. O. Willis, H. Lessure, and M. E. McHenry, Phys. Rev. B **42**, 2639 (1990).
[16] G. Blatter *et al.* (unpublished).
[17] V. N. Zavaritzky and N. V. Zavaritzky, Physica C **185–189**, 2141 (1991).
[18] T. Teruzzi, Ph.D. thesis, ETH Zürich, 1993.
[19] V. V. Metlushko, G. Güntherodt, I. N. Goncharov, A. Yu. Didyk, V. V. Moshchalkov, and Y. Bruynseraede, Physica B **194–196**, 2219 (1994).
[20] M. Nideröst, T. Teruzzi, R. Frassanito, A. Amann, P. Visani, and A. C. Mota, Physica C **235–240**, 2891 (1994).
[21] N. V. Zavaritzky, A. V. Samoilov, and A. A. Yurgens, Physica C **169**, 174 (1990).
[22] Stycast 1266, Grace N.V., 2431 Westerloo, Belgium.
[23] P. W. Anderson and Y. B. Kim, Rev. Mod. Phys. **36**, 39 (1964).
[24] A. C. Mota, A. Pollini, P. Visani, K. A. Müller, and J. G. Bednorz, Phys. Rev. B **36**, 4011 (1987).
[25] G. Blatter and V. Geshkenbein, Phys. Rev. B **47**, 2725 (1993).
[26] M. R. Beasley, R. Labusch, and W. W. Webb, Phys. Rev. **181**, 682 (1969).
[27] E. H. Brandt, J. Mod. Phys. B **5**, 751 (1991).
[28] P. W. Anderson, Phys. Rev. Lett. **9**, 309 (1962).
[29] V. B. Geshkenbein and A. I. Larkin, Sov. Phys. JETP **68**, 639 (1989).
[30] N. F. Mott, Philos. Mag. **19**, 835 (1969).
[31] B. I. Shklovskii and A. L. Efros, *Electronic Properties of Doped Semiconductors*, Springer Series in Solid-State Science No. 45 (Springer, Berlin, 1984).
[32] C. P. Bean, Phys. Rev. Lett. **8**, 250 (1962); Rev. Mod. Phys. **36**, 31 (1964).
[33] A. Gurevich and E. H. Brandt, Phys. Rev. Lett. **73**, 178 (1994).
[34] A. E. Koshelev and P. H. Kes, Phys. Rev. B **48**, 6539 (1993).
[35] R. Labusch, Phys. Status Solidi **19**, 715 (1967); **32**, 439 (1969); A. I. Larkin, Zh. Eksp. Teor. Fiz. **58**, 1466 (1970) [Sov. Phys. JETP **31**, 784 (1970)].
[36] C. P. Bean and J. D. Livingston, Phys. Rev. Lett. **12**, 14 (1964).
[37] A. M. Campbell and J. E. Evetts, *Critical Currents in Superconductors* (Taylor & Francis, London, 1972), p. 142.
[38] J. R. Clem, in *Proceedings of the 13th Conference on Low Temperature Physics*, edited by K. D. Timmerhaus, W. J. O'Sullivan, and E. F. Hammel (Plenum, New York, 1974), Vol. 3, p. 102.
[39] M. Konczykowski, L. I. Burlachkov, Y. Yeshurun, and F. Holtzberg, Phys. Rev. B **43**, 13 707 (1991); L. Burlachkov, *ibid*. **47**, 8056 (1993).
[40] E. Zeldov, A. I. Larkin, V. B. Geshkenbein, M. Konczykowski, D. Majer, B. Khaykovich, V. M. Vinokur, and H. Shtrikman, Phys. Rev. Lett. **73**, 1428 (1994).
[41] E. Zeldov, D. Majer, M. Konczykowski, A. I. Larkin, V. M. Vinokur, V. B. Geshkenbein, N. Chikumoto, and H. Shtrikman, Europhys. Lett. **30**, 367 (1995).
[42] A. I. Larkin and Yu. N. Ovchinnikov, Zh. Éksp. Teor. Fiz. **61**, 1221 (1971) [Sov. Phys. JETP **34**, 651 (1972)].
[43] R. P. Huebner, R. T. Kampwirth, and J. R. Clem, J. Low Temp. Phys. **6**, 275 (1972).
[44] G. Ries, H. W. Neumüller, and W. Schmidt, Supercond. Sci. Technol. **5**, 81 (1991).
[45] W. Paul, D. Hu, and Th. Bauman, Physica C **185–189**, 2373 (1991).
[46] A. Schilling, R. Jin, J. D. Guo, and H. R. Ott, Phys. Rev. Lett. **71**, 1899 (1993).
[47] M. Däumling, J. M. Seuntjens, and D. C. Larbalestier, Nature **346**, 332 (1990).
[48] V. N. Kopylov, A. E. Koshelev, I. F. Schegolev, and T. G. Togonidze, Physica C **170**, 291 (1990).
[49] G. Yang, P. Shang, S. D. Sutton, I. P. Jones, J. S. Abell, and C. E. Gough, Phys. Rev. B **48**, 4054 (1993).
[50] T. Tamegai, Y. Iye, I. Oguro, and K. Kishio, Physica C **213**, 33 (1993).
[51] Y. Yeshurun, N. Bontemps, L. Burlachkov, and A. Kapitulnik, Phys. Rev. B **49**, 1548 (1994).
[52] N. Chikumoto, M. Konczykowski, N. Motohira, K. Kishio, and K. Kitazawa, Physica C **185–189**, 2201 (1991).
[53] L. Krusin-Elbaum, L. Civale, V. M. Vinokur, and F. Holtzberg, Phys. Rev. Lett. **69**, 2280 (1992).